# Flexible Multifunctionalized Carbon Nanotubes-Based Hybrid Nanowires

*Nan Wang, Di Jiang, Lilei Ye, Murali Murugesan, Michael Edwards, Yifeng Fu, and Johan Liu**

**In this work, flexible multifunctionalized carbon nanotube (CNT)-based hybrid nanowires are synthesized through surface modification processes. The good dispersability of the hybrid nanowire in polar solvents facilitates directly making fine patterns with a minimum width of 40 μm for applications of flexible and stretchable circuits (FSCs). The hybrid nanowire possesses a flexible and highly conductive structure which demonstrates stable electro-mechanical properties on polydimethylsiloxane (PDMS) substrates under large structural deformation. FSCs fabricated from the hybrid nanowires show a constant resistance of 0.096 Ω □$^{-1}$ (equivalent of a resistivity 0.96 Ω μm) under repeated bending cycles. The FSCs also have a low and stable sheet resistance of 0.4 Ω □$^{-1}$ for strains up to 30%, which is almost four orders of magnitude lower than that of pure CNT samples (1316 Ω □$^{-1}$). Further improved stretchability and electro-mechanical properties (0.1 Ω □$^{-1}$, at the strain of 100%) are achieved with a prestrain PDMS substrate. Repeated deformation tests demonstrate the high reliability of FSCs. The observed stable and reliable electro-mechanical performance of FSCs suggests the potential use of the material in wearable and portable electronics.**

## 1. Introduction

As the demands of modern electronic systems call for increasing functionality, smaller system size, higher device connectivity, better user experience, and all at lower cost, flexible and stretchable circuits (FSCs) are becoming a high-growth technology in the area of electrical interconnects. This is due to their compact nature and high electrical-connection density over the traditional rigid printed circuit boards.[1] Comprising of a deformable substrate and conductive traces, FSCs possess an excellent deformation ability that will facilitate many new applications in the field of portable and wearable electronics, such as paper-like displays, smart clothing, stretchable solar cells, camera eyes, and biomedical sensors.[2–6] However, although the merits of FSCs are significant, there are some challenges that urgently need to be solved. One of the most critical points of this technology is the electro-mechanical reliability of the elastic interconnections, which are challenged in particular by relatively high and complex mechanical loading, such as, bending, compression, and elongation.[7]

Restricted by the demands of FSCs for high electro-mechanical performance, solutions to address the above problem are very challenging. Traditional strategies have been to use electroplated sinuous metallic wires deposited on deformable polymers, which had demonstrated high electrical conductivity under large tensile strains.[8,9] However, due to the lack of protection, the metallic wires usually suffer severe structural damage under repeated stretching/releasing cycles, which led to a poor reliability of FSCs and even complete failure. The recent development of patterning techniques has introduced alternative strategies for directly making FSCs patterns with a variety of highly conductive nanomaterials.[10,11] Kordás reported that elastic patterns of carbon nanotubes (CNTs) on a plastic film obtained a resistance of $R_s = 4 \times 10^4$ Ω □$^{-1}$ (resistivity of $4 \times 10^4$ Ω μm).[12] Wu fabricated a graphene electrode with a peak electrical performance of $R_s = 800$ Ω □$^{-1}$ (resistivity of 5.6 Ω μm).[13] Hu achieved a minimum resistance of $R_s = 50$ Ω □$^{-1}$ (resistivity of $2 \times 10^2$ Ω μm) with a transparent and flexible silver nanowire-based electrodes.[14] However, some challenges raised from the material themselves still limit their applications; carbon-based nanomaterials, like pristine CNTs and graphene, can easily form agglomerations that are hard to disperse. This makes it difficult to form uniform patterns, and their relatively high contact resistance to metals might also lead to the poor electrical performance of FSCs. Metal nanowires lack flexibility and suffer structural damage at large strain that can cause the complete failure of FSCs. To satisfy the requirements for developing FSCs with stable electro-mechanical properties and high reliability, it is therefore desirable to synthesize hybrid nanomaterials that possess the high conductivity of metals together with good flexibility and dispersability.

N. Wang, D. Jiang, Dr. M. Murugesan,
Dr. M. Edwards, Prof. J. Liu
Department of Microtechnology and Nanoscience (MC2)
Chalmers University of Technology
Kemivägen 9, SE 412, 96 Göteborg, Sweden
E-mail: johan.liu@chalmers.se
Dr. L. Ye, Dr. Y. Fu
SHT Smart High-Tech AB
Aschebergsgatan 46, SE-411, 33 Göteborg, Sweden
Prof. J. Liu
SMIT Center and School of Mechatronics and Mechanical Engineering
Key Laboratory of New Displays and System Integration
Shanghai University No 149
Yan Chang Road, Shanghai 200072, China

**DOI: 10.1002/adfm.201501017**

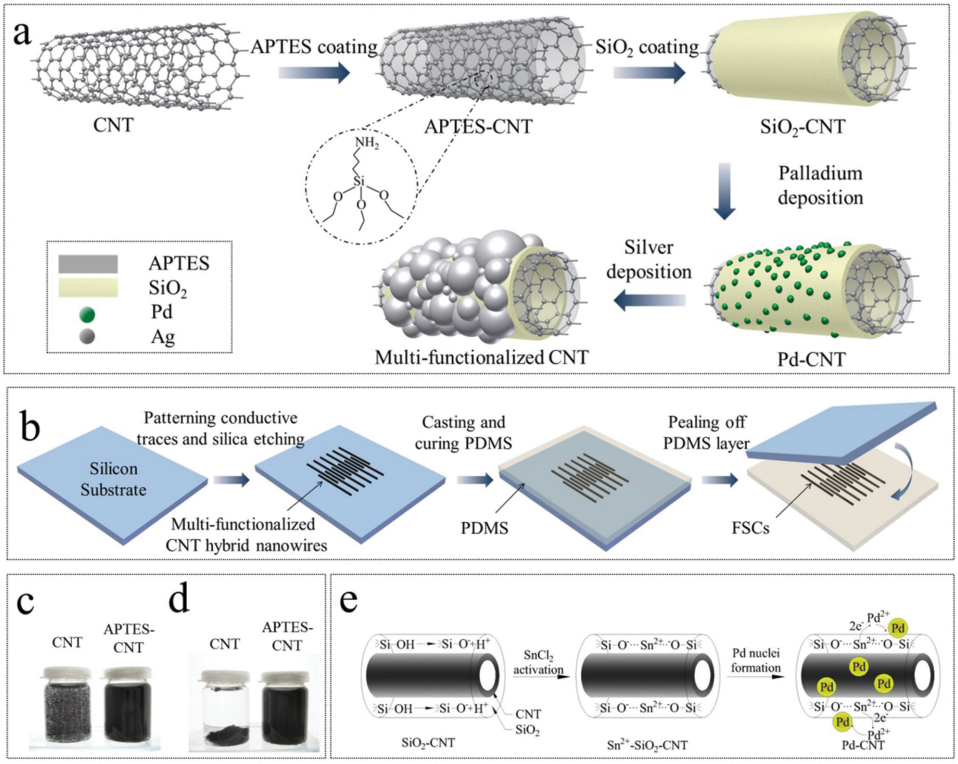


**Figure 1.** a) Schematic of the various modification steps in the synthesis of multifunctionalized CNT-based hybrid nanowires. The surface of CNTs was coated with APTES, silica, palladium nanoparticles, and silver nanoparticles. b) Schematic of the preparation of FSCs based on the hybrid nanowires and PDMS. c) Dispersion of CNTs in ethanol before and after APTES coating. A homogeneous CNTs ethanol solution was obtained after modification with APTES. d) Solution stability of CNTs in ethanol without and with APTES coating for the period of one month after preparation. No delamination or sediment was detected in the ethanol dispersion of APTES-CNTs. e) Reaction mechanism of palladium nanoparticles deposition in silica layer.

In this work, a new surface modification process for synthesizing intrinsically flexible multifunctionalized CNT-based hybrid nanowires and its application in the field of FSCs is presented. The key benefit of the hybrid nanowire lies in their high electrical conductivity and flexible structures to maintain stable electrical and mechanical performances under significant structural deformation. The multifunctionalized CNT-based hybrid nanowires are synthesized with different functional materials on the surface of CNTs to produce a metal nanoparticle coating layer and form uniform dispersions whilst possessing the CNT's original structural integrity and high flexibility. The FSCs based on the hybrid nanowires embedded in polydimethylsiloxane (PDMS) substrate demonstrated a highly stable and low sheet resistance of 0.096 $\Omega\ \square^{-1}$ (resistivity of 0.96 $\Omega$ μm) under repeated bending tests together with a relatively stable sheet resistance of 0.40 $\Omega\ \square^{-1}$ (resistivity of 4 $\Omega$ μm) within a stretching ratio of 30%. The stretchability and electrical stability of the FSCs can be further improved till to 0.1 $\Omega\ \square^{-1}$ (resistivity of 1 $\Omega$ μm) at a strain ratio of 100% with prestretched PDMS substrates. Reliability tests of repeated stretching and bending were carried out using a high precision load/displacement measurement machine and identified the good electrical reliability of FSCs. Morphology study has proved that the hybrid nanowires possess a flexible structure which is essential for the stable electro-mechanical performance of FSCs under large structural deformation. Importantly, the multifunctionalized CNT-based hybrid nanowires are able to disperse in various polar solvents and form homogenous suspensions that facilitate making uniform and fine structures with existing patterning techniques. These results facilitate the fabrication of high-resolution FSCs with stable electro-mechanical properties. Light-emitting diodes (LED) demonstrators were also made to illustrate the mechanical strength and electrical performance of multifunctionalized CNT-based FSCs.

## 2. Results and Discussions

The fabrication processes of multifunctionalized CNT-based hybrid nanowires are schematically illustrated in **Figure 1**a. The surface of CNTs was successively coated with first a cross-linked (3-aminopropyl)triethoxysilane (APTES) layer, then a silica layer, followed by palladium nanoparticle and silver nanoparticle deposition. Every functional material in a hybrid nanowire has been specifically chosen for its beneficial properties: CNTs act as a flexible framework as well as additional electron pathways. APTES improves the dispersion of CNTs in polar solvents through bringing in hydrophilic silane and amino groups on the surface of CNTs. The mesoporous silica layer is used as templates for the attachment and deposition of metallic nanoparticles. Palladium nanoparticles served as catalysts to provide nucleation sites for silver growth. Finally, silver nanoparticles are the main conductive media to improve the contact surface

of the hybrid nanowires and build high-efficiency conductive networks.

Pristine CNTs have very large aspect ratios and highly inertial surfaces, which make them uneasy to form homogeneous and stable dispersion. To address such a challenge, the required surface activation of CNTs needs to be carried out. In previous reports, this was generally achieved through an oxidation pretreatment of CNTs or surfactant assisted separation processes.[15,16] However, such treatments always lead to severe structural damage as well as poor electrical and mechanical performance to CNTs. In this work, CNTs were coated with a cross-linked APTES polymer layer (APTES-CNTs). The large amounts of hydrophilic groups of APTES, such as Si—OH and —$NH_2$, would assist CNTs to be homogeneously dispersed in polar solvents. Importantly, the APTES layer can be completely removed in the follow-up process without having any adverse effects on the CNT's properties. The reaction mechanism of forming APTES-CNTs is schematically illustrated in Figure S1 (Supporting Information). CNTs exhibit a negatively charged surface in ethanol at high pH value (pH > 7), which can attract the positively charged APTES monomer through electrostatic absorption.[17] The attracted APTES monomers cross linked with each other under alkaline conditions and formed a coating layer on the surface of CNT. Figure 1c shows the difference of the CNT dispersions in ethanol before and after APTES coating. A homogeneous CNT ethanol solution was obtained after functionalizing with APTES. Additionally, the APTES-CNT suspension exhibits good stability for the period of one month after preparation (Figure 1d). No sediments were detected in the ethanol dispersion of APTES-CNTs, which indicates the effectiveness of the APTES coating onto the CNT surfaces.

After being functionalized with APTES, silica coating was carried out onto the surface of the CNTs ($SiO_2$-CNTs) through the hydrolysis reaction of tetraethyl orthosilicate (TEOS) under alkaline conditions to act as templates for metal nanoparticles deposition.[18] Fourier-transform infrared spectroscopy (FTIR) was employed to confirm both the attachment of APTES and formation of $SiO_2$ around the composite (Figure S2, Supporting Information). The peaks at 1700 and 2900 $cm^{-1}$ corresponding to C—O and C—H groups indicate that the CNT has defects due to the production processes used by the CNT supplier. After functionalizing with APTES, the peaks corresponding to Si—OH stretching and asymmetric Si—O—Si stretching appeared at 980 and 1080 $cm^{-1}$, respectively. Moreover, a broad band located between 3400 and 3500 $cm^{-1}$ represents N—H stretching of the amino group in APTES. After TEOS treatment, the peak corresponding to Si—O—Si stretching becomes stronger due to the formation of a silica layer.

Transmission electron microscopy (TEM) study was carried out to understand the morphology changes of CNTs before and after the silica coating process. The image of pure CNTs shown in **Figure 2**a indicates a smooth surface with a diameter of 10 nm. In comparison, a shell structure along the axial direction of the nanotubes can be observed from Figure 2b, which indicates a successful silica coating on the CNT. The thickness of the silica shell was found to be about 10 nm which can be varied through changing the concentration of TEOS. The impact of the APTES layer to the silica coating was also examined via a control experiment of coating the silica directly on CNTs without APTES modification layers. It has been found that the deposition of $SiO_2$ was random and individual CNTs tended to form big bundles (Figure 2c). Therefore, it can be deduced that APTES layer not only assisted the dispersion of CNTs but also acted as an adhesion layer for the silica coating process.

The $SiO_2$ layer exhibits a strong binding ability with positively charged ions due to the attraction of Si—OH group and also a mesoporous structure which would facilitates the targeted metal nanoparticle growth.[19,20] Figure 1e illustrates the deposition of palladium nanoparticles on CNT (Pd-CNTs). Metallic palladium (Pd) nanoparticles were generated

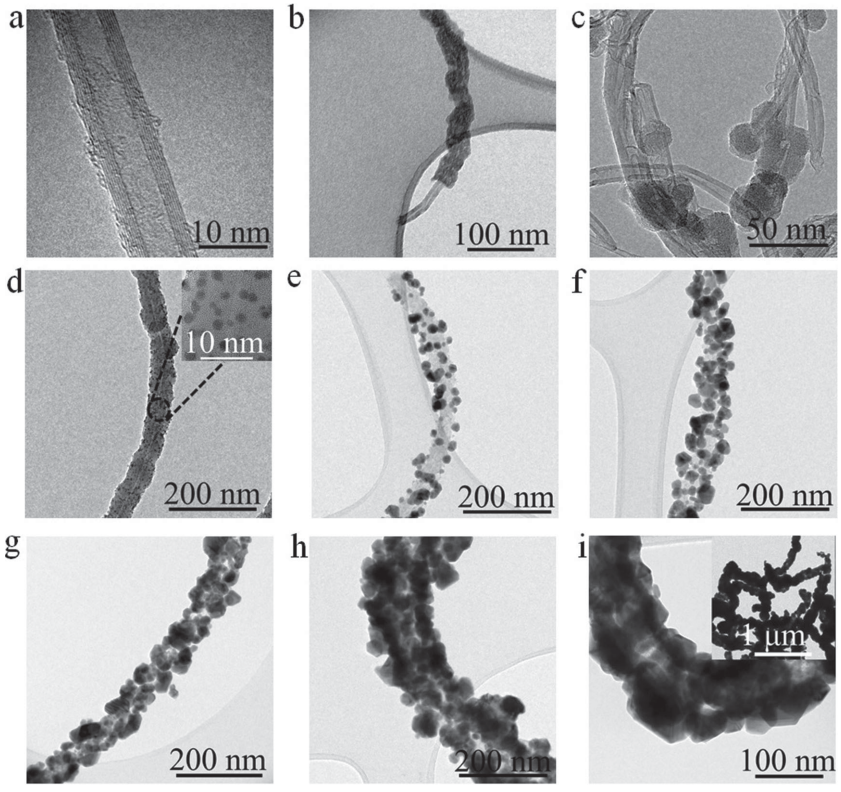


**Figure 2.** a) A pure CNT with a diameter of 10 nm. b) $SiO_2$-CNTs. An amorphous silica layer with a thickness about 10 nm was deposited at the surface of APTES-CNTs. c) Control experiment of silica coating directly on CNTs without APTES modification. A random and unselective $SiO_2$ deposition on CNTs with huge bundles was observed. d) Pd-CNTs. Dense and uniform palladium nuclei were deposited in silica layer and no free particle were observed. The inset shows that the average size of palladium nuclei is about 3 nm. e–i) Multifunctionalized CNT-based hybrid nanowires prepared with different silver nitrate concentrations: e) 1 g $L^{-1}$; f) 2 g $L^{-1}$; g) 5 g $L^{-1}$; h) 10 g $L^{-1}$; i) 15 g $L^{-1}$, the inset shows the zoom out image of hybrid nanowire connection.

through the reduction of $Pd^{2+}$ ions by $Sn^{2+}$ ions which were pretrapped in the silica layer. TEM image in Figure 2d shows the morphology change of CNT after palladium deposition. A large quantity of Pd nanoparticles with an average particle size of 3 nm was uniformly deposited in the $SiO_2$ layer. Those Pd nanoparticles would act as nucleation sites for the proceeding silver growth on CNTs. Finally, multifunctionalized CNT-based hybrid nanowires were obtained through electroless silver plating. Mild reaction conditions were maintained during silver nanoparticle growth to ensure the uniform and complete silver deposition on the CNTs. The degree of silver nanoparticles coverage on the CNT surfaces was found to be very critical for optimizing the electrical performance of the hybrid nanowires. Hence, a series of multifunctionalized CNT specimens were prepared with increased silver nitrate concentrations from 1 to 15 g $L^{-1}$ to study the effect of silver nitrate concentration on the metallic coverage of the CNTs. TEM observation shows that the morphologies of the CNTs changed as the silver nitrate concentrations were varied (Figure 2e–i). When a lower silver nitrate concentration (1 g $L^{-1}$) was used, small silver nanoparticles with an average size of 20 nm were formed due to presence of inadequate silver precursor sources (Figure 2e). Upon increasing the concentration of silver nitrate from 1 to 10 g $L^{-1}$, the average size of silver nanoparticles was increased from 20 to 50 nm with an enlarged surface coverage (Figure 2f–h). When the silver nitrate concentration reaches to 15 g $L^{-1}$ (Figure 2i), a layer of densely packed silver nanoparticles was formed around the whole CNTs surface. No free silver nanoparticles or obvious agglomerations were detected after using a higher silver nitrate concentration. The X-ray diffraction (XRD) pattern of Ag-CNTs hybrid nanowires (Figure S3, Supporting Information) indicates that the silver nanoparticles deposited over the CNT surface have a highly pure crystallinity. These results show advantages of our process on both protecting CNT's structure and coating complete metallic nanoparticle layers compared with the previous reports.[21–23]

Owing to the presence of abundant hydrophilic groups, such as Si—OH and $NH_2$, the as-fabricated multifunctionalized CNT-based hybrid nanowires were found to be easily dispersed in various polar solvents and form homogenous suspensions (Figure S4, Supporting Information). UV–vis spectroscopy analysis further shows that the hybrid nanowire ethanol dispersions have good uniformity and stability (Figure S5, Supporting Information). These results made it possible to fabricate FSCs with uniform structures via direct patterning processes. In this work, a mask patterning process was developed and utilized for FSCs fabrication, which is schematically illustrated in Figure 1b. The prepared hybrid nanowire ethanol dispersion were filtrated and deposited onto silicon substrates through patterning of a shadow silicon mask. After removing the mask, the deposited structure on the substrate was then washed with a diluted hydrofluoric acid (HF) solution and dried in air to both completely remove all forms of silica (both APTES and silica layers) and restore the flexibility and conductivity of multifunctionalized CNT-based hybrid nanowires. FTIR tests were carried out for multifunctionalized CNT samples before and after HF etching, results were shown in Figure S6 (Supporting Information). Two characteristic peaks at 1000 $cm^{-1}$ corresponding to Si—O—Si and Si—OH groups disappeared after HF etching of the multifunctionalized CNT-based hybrid nanowires, which identified the complete removal of the silica layer. Moreover, no other characteristic peaks were found after HF etching indicates that the surface modification process and the HF etching process had no effect to the structure of CNTs. Figure S7 (Supporting Information) shows the TEM image of CNT-based hybrid nanowires after HF etching. It has been found that the hybrid nanowires still retain a complete silver nanoparticle coating layer after removing both the silica and APTES layer by HF etching. PDMS was then cast onto the top of the silicon substrate and infiltrated through the gap in the patterned structures to provide mechanical support. After curing, the PDMS layer was peeled off from the substrate. The conductive traces were embedded below the PDMS surface to form conductive FSCs. **Figure 3**a shows parallel patterns of a 20-wire array with each wire having a length of 15 mm and a width of 500 μm. The effect of thickness variation to the resistivity change was also studied. As shown in Figure S8 (Supporting Information), different conductive traces with different thicknesses ranging from 5 to 15 μm were fabricated, and their respective resistivity and sheet resistance were plotted by the four-probe method. The resistivity was found to be almost constant in this range, which indicates good interconnection of the individual hybrid nanowires. Therefore, the thickness of patterned conductive traces was regulated around 10 μm through controlling the volume of the solution to give stable electro-mechanical properties and ensuring the good reliability of the FSCs. In the following discussion, sheet resistance for 10 μm thick traces will be used as the main electrical performance indicator. The average thickness of PDMS substrate is 500 μm. The inset in Figure 3a shows FSCs at the bending state. It can be seen that the conductive line remains both continuous and uniform when rolled up till 180°, with no indication of breakage or voids. Figure 3b shows another example of FSCs with different patterns. Each unit of FSCs consists of line structures with varied widths and the minimum width demonstrated in the unit is 40 μm (Figure S9, Supporting Information). It shows the potential ability of multifunctionalized CNT-based hybrid nanowires for fine patterning.

The degree of silver nanoparticle coverage on CNT surfaces plays a crucial factor in the electrical performance of FSCs. To study this effect, different FSC samples were prepared by using multifunctionalized CNT-based hybrid nanowires with varied degrees of silver coverage ($C_{AgNO3}$ = 0–15 g $L^{-1}$). The sheet resistance of each sample was tested by the four-probe method and results were shown in Figure 3d. It has been found that the sheet resistance of FSCs decreases rapidly with increasing silver nitrate concentrations, compared to the reference sample made from pure CNTs (1316 Ω □$^{-1}$, resistivity of $1.3 \times 10^4$ Ω μm). For samples prepared with silver nitrate concentrations of 1, 2, 5, and 10 g $L^{-1}$, the sheet resistance values are 100.81, 4.07, 0.38, and 0.15 Ω □$^{-1}$, respectively, and the percolation threshold for an exponential decrease in resistance was located at 2 g $L^{-1}$. It indicates that silver nanoparticles at the CNT surface were interconnecting and provide the main contribution to electrical conductivity when the silver nitrate concentration reached 2 g $L^{-1}$. The minimum sheet resistance (0.096 Ω □$^{-1}$, resistivity of 0.96 Ω μm) was reached when CNTs were fully covered with silver nanoparticles ($C_{AgNO3}$ = 15 g $L^{-1}$),

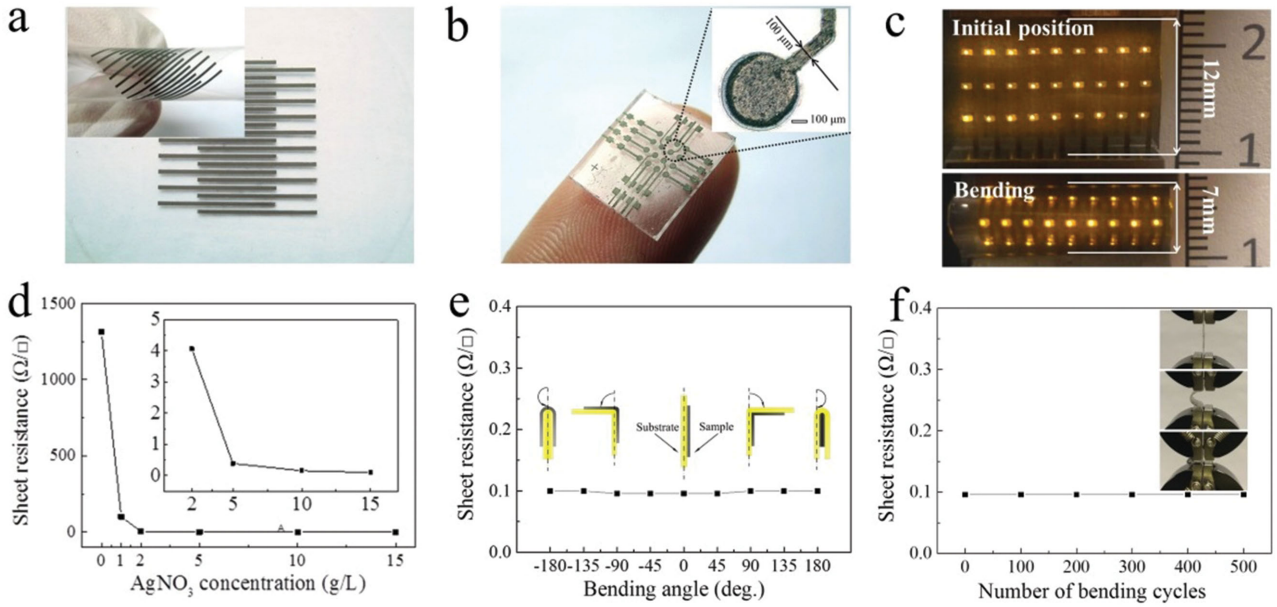


**Figure 3.** a) FSCs with 10/10 lines, each line has a length of 1.5 cm and a width of 500 μm. The insets show the optical images of bent (180°). b) Optical image of FSCs (8 mm × 8 mm) with a minimum diameter of 100 μm, which indicates the ability of multifunctionalized CNT hybrid nanowires for making arbitrary and fine patterns. c) Optical images of LED array integrated at FSCs with and without bending. LEDs remained lit with the same illumination intensity as at 0% strain when the demonstrator was bent to 180°. It indicates the stable electrical performance of the FSCs. d) Electrical tests show a decrease of sheet resistance with the increase of silver nanoparticles coverage on CNT. A minimum resistance of 0.096 Ω □$^{-1}$ (equivalent resistivity of 0.96 Ω μm) at 0% strain was obtained when CNT was totally covered by silver. e) The sheet resistance change of FSCs ($C_{AgNO3}$ = 15 g L$^{-1}$) as a function of bending angle. A small variation of sheet resistance less than 3.8% was observed when FSCs were bent up to 180°, which indicated the stable electro-mechanical properties of FSCs. f) Resistance results of FSCs upon bending cycles. FSCs demonstrate a high reliability after 500 cycles of bending/releasing.

which means that a complete silver nanoparticle coating layer can minimize the contact resistance and provide sufficient conductive channels inside the conductive traces. These results are consistent with the morphology change of multifunctionalized CNT-based hybrid nanowires as observed in Figure 2e–i. Moreover, high temperature annealing can further decrease the sheet resistance of the conductive traces due to the sintering of silver nanoparticles. However, a rigid silver shell can hinder the flexibility of the hybrid nanowires, which would lead to a poor electro-mechanical performance under large structural deformation.

The bending effect on the sheet resistance of FSCs comprising of multifunctionalized CNT-based hybrid nanowires ($C_{AgNO3}$ = 15 g L$^{-1}$) was investigated further on a high precision load/displacement measurement machine with a strain rate of 5 mm s$^{-1}$. Figure 3e shows the sheet resistance variation of FSCs as a function of bending angles (–180°–180°). Notably, a small variation of resistance less than 3.8% was observed when the sample was bent up to 180°, and it recovered after straightening. Notably, after 500 cycles for a bending angle of 180°, the electrical resistance remained constant, as shown in Figure 3f. These results show the excellent electro-mechanical stability of hybrid nanowires during bending tests compared with conventional materials used in flexible electronics, even graphene which shows a resistance increase of 20% after the third bending cycle due to the crack formation.[24] The microstructural analysis of the FSCs further helps to understand the reasons for their outstanding electrical performance. As shown in Figure S10a (Supporting Information), the hybrid nanowires entangled with each other to form a conductive network after patterning and acted as the main electron pathways for FSCs. Figure S10b (Supporting Information) shows the surface morphology of FSCs after PDMS infiltration. It can be seen that PDMS has penetrated through the conductive layer and filled all along the inside gaps of the conductive network. The complete filling of PDMS provides enough mechanical support for absorbing stresses and protecting the multifunctionalized CNT-based hybrid nanowires from structural damages under large deformation. To demonstrate the electrical resistance change of FSCs during bending, an array of LEDs was assembled on the top of the parallel wires and sealed with PDMS layer. Figure 3c shows the lit image of LEDs before and during bending. It was found that LED demonstrators showed the same illumination intensity at the bending state as the initial state, which indicates the stable electrical performance of FSCs. This result was also consistent with the bending test (Figure 3e).

The electrical performance of FSCs ($C_{AgNO3}$ = 15 g L$^{-1}$) was also investigated as a function of tensile strain on the high precision load/displacement measurement machine at the same strain rate of 5 mm s$^{-1}$. **Figure 4**a shows the results at a maximum strain of 60%. During the first stretching/releasing cycle, the resistance remained stable (≈0.1 Ω □$^{-1}$) under 30% stretching. Further increasing the tensile strain to 60%, the resistance showed an obvious increase from 0.1 to 0.96 Ω □$^{-1}$. Upon the release of the strain, the sheet resistance was partially recovered and stabilized at 0.35 Ω □$^{-1}$ with 0% strain. After

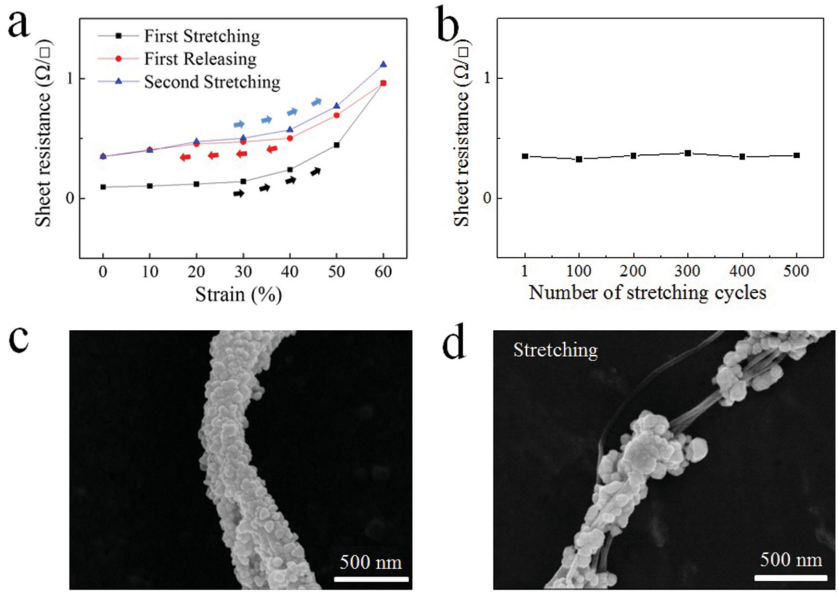


**Figure 4.** a) Resistance change of FSCs ($C_{AgNO3}$ = 15 g $L^{-1}$) as a function of applied strains. The resistance remained stable (≈0.1 Ω □$^{-1}$) under 30% stretching. Further increasing the tensile strain to 60%, the resistance showed an increase from 0.1 to 0.96 Ω □$^{-1}$. Upon the release of the strain, the sheet resistance was partially recovered and stabilized at 0.35 Ω □$^{-1}$ with 0% strain. b) Reliability of FSCs under repeated stretching/releasing cycles. After the first stretching/releasing cycle, FSCs showed a stable sheet resistance (0.35 Ω □$^{-1}$ at 0% strain) with less than 8% variation after 500 repeated cycles. c) SEM images of the multifunctionalized CNT-based hybrid nanowire after HF etching. The hybrid nanowire still holds a complete silver-nanoparticle layer even though some defects were identified. d) When a small tensile strain (<30%) was applied, the original bent hybrid nanowires was firstly straighten toward the direction of strain, which showed stable electro-mechanical properties of FSCs within 30% strain. With the strain ratio further increasing till 60%, the silver-nanoparticles layer was broken to short pieces and they had a shift along the axis of CNTs toward the direction of stretching. The interspaces between each piece prevent further structural damage. Moreover, it can be seen that CNT bundles have a close connection with each silver piece after removing APTES and silica layers and act as bridges to provide more pathways for electron transmission.

the first cycle of stretching/releasing, the electrical resistance was restored to a stable value, with a resistance increase of ≈30% under 30% stretching. The stable electrical performance under 30% of strain indicates that it can be intrinsically attributed to the reserved elongation of the hybrid nanowires due to their flexible and curved structures (Figure 2i). Moreover, the obvious resistance increase could be caused when strain ratio exceeded 60% due to the partially breaking or cracking of the silver nanoparticle layer on CNT's surface, which can possibly lead to an electrical breakdown. Mechanical breakage of FSCs took place when PDMS was stretched beyond the maximum elongation ratio of 100%. Additional stretch/release cycles in the range of 0%–60% were performed to evaluate the reliability of FSCs. For up to 500 repeated stretching cycles, FSCs showed relatively stable sheet resistance (0.35 Ω □$^{-1}$ at the strain of 0%) with a small variation of less than 8% (Figure 4b), with no observed indication of failure. These results demonstrate good reliability and stable electro-mechanical properties of the hybrid nanowire-based FSCs when compared to other reported CNT and silver nanowire composites.[25–27] For example, many of single-walled carbon nanotube flexible composites showed order-of-magnitude higher initial resistivity and significant increase of resistance after the first stretching cycle due to the large contact resistivity of individual CNTs.[25,26] Furthermore, the stretchable electrode based on a silver nanowire-polymer composite presented a poor electro-mechanical stability for stretching (1000 times increase of resistivity at the strain of 80%) and low reliability under strain cycles (three times increase of resistivity at the first 500 cycles with a strain of 30%) due to the detachment of the nanowire contacts and crack formation during stretching.[27]

In order to understand the electrical conduction mechanism of FSCs, morphology analysis of the multifunctionalized CNT-based hybrid nanowires before and under stretching was performed by scanning electron microscopy (SEM), with the results shown in Figure 4c,d. It can be seen that the multifunctionalized CNT-based hybrid nanowires still retain a complete silver nanoparticle coating layer after removing both the silica and APTES layer by HF etching. Subsequently when the FSCs were stretched, the original bent hybrid nanowires were straightened toward the direction of the tensile strain. The bent structure of the hybrid nanowires helps to maintain a stable electrical resistance of FSCs within a tensile strain of 30%. With further increase of the tensile strain, the original silver nanoparticles layer was broken into short pieces that had moved along the axis of CNTs toward the direction of tensile strain. The breakage of the silver nanoparticle coating layer led to the increase of resistance beyond a strain ratio of 30%. However, more stretch/release cycles did not cause a complete failure or any further resistance increase in the FSCs. It has been found that these short pieces were still attached to the surface of CNTs after stretching, instead of forming individual nanoparticles. Under large strains, the interspaces between each piece had enough room for their movement, preventing further structural damage. Moreover, the network of CNTs still acted like bridges to connect each piece and provide more pathways for electron transmission. This also partially helped to maintain a low resistance of FSCs at larger strains.

To further improve the electrical stability as well as the stretchability, FSCs were transferred onto a prestretched PDMS substrate with a tensile strain of 100%. The sheet resistance of the sample was evaluated and shown in **Figure 5**a. It has been found that FSCs showed a stable sheet resistance (≈0.1 Ω □$^{-1}$) with a small variation of 7% under 100% stretching. This result represents a threefold of improvement in the electro-mechanical properties of FSCs compared to the previous case when the nonprestretched FSC was strained to 30%. Such stable electro-mechanical performance of FSCs is attributed to the highly flexible structure of the hybrid nanowires and protection of PDMS. Further increase of the prestrain ratio of the PDMS substrate could result in an even more stable electrical

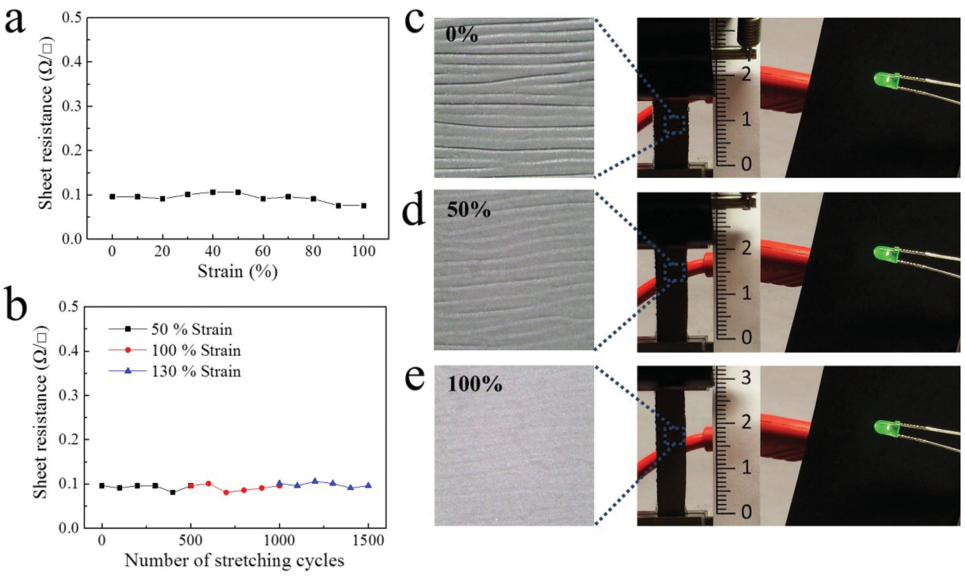


**Figure 5.** a) Resistance change of FSCs on the prestretched silicon rubber substrate as a function of applied strain. FSCs showed a highly stable sheet resistance (≈0.1 Ω □$^{-1}$) with a small variation of 7% under 100% stretching. Such stable electro-mechanical properties are attributed to the flexibility of the hybrid nanowires. b) Resistance results of FSCs on the prestretched silicon rubber substrate under repeated stretch and release cycles. During the first 500 cycles, the FSCs were stretched with 50% strain and showed a constant resistance ($R/R_0 \approx 1$ at 0% strain), and for the second 500 cycles, FSCs were stretched to an increased strain ratio of 100% and also showed a stable resistance ($R/R_0 \approx 1$ at 0% strain). At the last 500 cycles, FSCs were stretched with a further increased strain of 130%. The resistance still remained stable with a slight increase of 10% ($R/R_0 = 1.1$ at 0% strain). c–e) LED demonstrator and surface morphology change of FSCs under stretching (see video S1, Supporting Information). Compared to the initial light state (strain = 0%), the LED demonstrator remained the same illumination intensity under different stretching ratios (50% and 100%). The optical image of the conductor surface showed that some wrinkles appear against the direction of stretching at the initial state and disappear as the strain decreased. The good reliability of the FSCs on the prestretched substrate was attributed to the excellent flexibility of hybrid nanowires and the sufficient protection from PDMS.

performance and improved stretchability. Moreover, the maximum strain was increased to 800% before causing mechanical breakdown of prestretched FSCs due to the use of even softer PDMS (ELASTOSIL®RT 4600A/B). The electrical reliability test was also carried out on the high precision load/displacement measurement machine with a strain rate of 5 mm s$^{-1}$ to evaluate the reliability of FSCs on the prestretched silicon rubber substrate, with the results shown in Figure 5b. During the first 500 cycles, the FSCs were stretched with 50% strain and showed a constant resistance ($R/R_0 \approx 1$ at 0% strain), and for the second 500 cycles, FSCs were stretched to an increased strain ratio of 100% and also showed a stable resistance ($R/R_0 \approx 1$ at 0% strain). At the last 500 cycles, FSCs were stretched with a further increased strain of 130%. The resistance still remained stable with a slight increase of 10% ($R/R_0 = 1.1$ at 0% strain). Such stable electrical performance of the FSCs is attributed to the intrinsic flexibility of the multifunctionalized CNT-based hybrid nanowires and the sufficient protection from the PDMS layer. These results indicate the stable and superior electro-mechanical properties of FSCs under larger stretching ratios compared to other reports on elastic conductors in literature.[9,26–35] For example, electronic whiskers based on patterned carbon nanotube and silver nanoparticle show a three times increase in resistance at a small strain of 2.4% due to the increase of distance between individual silver nanoparticles.[28] Prestretched PDMS substrate with copper coating suffer poor reliability caused by cracks formation during repeated stretching/releasing cycles.[9] Stretchable conductors comprising of silver nanowires suffer an irreversible increase of resistance after the first stretch/release cycle due to the rigid structure of silver nanowires, and they also show poor electro-mechanical performance and low electrical stability.[27,29] Many metal/polymer composite films exhibit lower reliability than the hybrid nanowire-based FSCs.[30–32] A variety of reported FSCs comprising of CNTs and elastic polymers show resistance that are orders of magnitude higher than that of multifunctionalized CNT-based hybrid nanowires based FSCs.[26,33–35]

A LED demonstrator was built to illustrate the resistance change of the FSCs on a prestretched PDMS substrate, which was stretched at different strain ratios with the assist of high precision load/displacement measurement machine. Figure S11 (Supporting Information) shows the schematic of the circuit of the LED demonstrator comprising of the conductive trace fixed between two clamps of the load/displacement machine, an LED and power source. The conductive trace was cyclically stretched with a strain rate of 5 mm s$^{-1}$. The working voltage of the LED is 2 V. The lit images and the surface morphology of the conductive trace are shown in Figure 5c–e. Compared to the initial light state (strain = 0%), the LED remained the same brightness under different strain ratios (50% and 100%). Due to the prestretched PDMS substrate, the surface of conductor showed some wrinkles running opposite to the direction of stretching in the initial state (0% strain) and these started to disappear as the percentage strain was increased. Those wrinkles would raise challenges to the direct connection between conductive wires and functional devices. Therefore, it

is essential to combine both nonprestretched and prestretched FSCs for meeting various requirements of real applications. The sufficient protection from the PDMS layer prevented the conductive layer from getting any structural damage. Video of LED (video S1, Supporting Information) lit effect under ten cycles of stretching/releasing is also available in the Supporting Information.

## 3. Conclusion

In this work, CNTs were functionalized with various coating layers including APTES, mesoporous silica and silver nanoparticles to form the multifunctionalized CNT-based hybrid nanowires, which demonstrated very low electrical resistivity, high flexibility, and stretchability. Notably, the hybrid nanowires can form homogeneous dispersions in various polar solvents, which facilitate forming fine structures with many existing patterning techniques. FSCs based on hybrid nanowires showed stable electro-mechanical properties and high reliability in both bending test and stretching test under 30% of strain. The stretchability and electrical stability could be further improved by utilizing a prestretched PDMS substrate. These results indicate the great potential of the hybrid nanowire in many applications including wearable flexible displays, stretchable energy generators and capacitors, electronic skins, deformable sensor, and actuator applications.

## 4. Experimental Section

*Materials*: Multiwall CNTs with a mean diameter of 15 nm were obtained from TIMENANO, China and ultrasonically cleaned in an ethanol solution before use. APTES (99%), polyvinylpyrrolidone (PVP, average $M$ = 10 000 g $mol^{-1}$), TEOS (98%,), palladium(II) chloride (99%), tin(II) chloride (98%), silver nitrate (99%), ammonium hydroxide solution (28%), glucose (99.5%), tartaric acid (99.5%), sodium hydroxide (98%), and hydrofluoric acid (48 wt%) were purchased from Sigma-Aldrich. PDMS with elongation ratios of 100% and 800% (ELASTOSIL RT 601A/B and 4600A/B) were purchased from Wacker Chemie, Germany. Absolute ethanol (99.9%) was purchased from VWR International. Other reagents and solvents were used as received and without further purification.

*Preparation of Multifunctionalized CNTs Hybrid Nanowires*: CNTs were first dispersed into $8 \times 10^{-3}$ M APTES ethanol under ultrasonication for 10 min to get APTES monomer attached onto the surface of CNTs, and then, the solid was vacuum filtrated and rinsed with ethanol to completely remove extra APTES which was not attached on the surface of CNTs. The dried CNTs were transferred into an ethanol solution with 2 mg $mL^{-1}$ PVP (dispersing agent), followed by ultrasonication in a water bath for 30 min to obtain a stable and homogeneous suspension. An appropriate amount of aqueous ammonia was quickly added to the above solution to adjust the solution's pH value to 10. The cross-linking of APTES at the surface of CNTs was carried out at room temperature. After 6 h, the mixture was filtrated and rinsed three times with ethanol to remove PVP completely. The silane modified CNTs (APTES-CNTs) were dispersed into a solution with 100 mL ethanol, 2 mL TEOS, and 5 mL concentrated aqueous ammonia under ultrasonication. The coating of silica on CNTs was carried out at room temperature for 6 h. After reaction, the solution was centrifuged at 3000 rpm to fully remove free silica particles, and the silica coated CNTs were collected. The mixture was rinsed thoroughly with ethanol and dried at 60 °C in a vacuum oven. The thickness of the silica coating can be modified by changing the reaction time and the concentration of TEOS. The CNTs after silica coating were named $SiO_2$-CNTs. The purified $SiO_2$-CNTs were dispersed into 2 g $L^{-1}$ $SnCl_2{\cdot}2H_2O$ (sensitizing agent) aqueous solution for 20 min under a mild stirring condition. Then the mixture was vacuum filtrated and washed three times with distilled water. The $Sn^{2+}$ sensitized CNTs were dispersed into 1 g $L^{-1}$ $PdCl_2$ aqueous solution to deposit palladium seeds onto the silica layer, which are referred to after the process as Pd-CNTs. After the reaction, the Pd-CNTs were collected and purified through filtration and washing. They were kept at 60 °C under vacuum for more than 3 h to completely remove the water. Then Pd-CNTs were dispersed into a freshly prepared electroless bath solution (pH = 8.5) containing silver complex ($4.25 \times 10^{-3}$ M $Ag(NH_3)^{2+}$) and a reducing agent consisting glucose ($2.27 \times 10^{-2}$ M), tartaric acid ($2.67 \times 10^{-3}$ M), and ethanol (1.7 M). To enhance the stability of the plating solution, the reducing solution was boiled for 10 min to thoroughly convert the glucose molecules into an inverted sugar before mixing with the silver complex solution. The whole reaction was carried out at room temperature with mild stirring condition. After 6 h, the CNTs-based composite was separated, rinsed thoroughly with distilled water, and dried at 60 °C in a vacuum oven. The final CNTs-based composite is referred to as multifunctionalized CNT-based hybrid nanowires in this work.

*Preparation of FSCs and LED Demonstrator*: FSCs based on multifunctionalized CNT-based hybrid nanowires were fabricated through a mask patterning process. Multifunctionalized CNT-based hybrid nanowires were dispersed into ethanol and formed dispersion with a concentration of 7 mg $mL^{-1}$. Desired patterns of FSCs could be achieved by filtration of the above dispersion through a patterned mask. To achieve a high resolution, two pieces of hollow silicon wafer with same patterns were stacked onto the each side of a filter (pore size = 0.8 μm) and formed a sandwich structure. One silicon wafer acted as the substrate to hold the patterned FSCs and the other was the mask. By using such a structure, the hybrid nanowire dispersion can only be filtrated through the hollow areas of two masks without spreading to the places on the filter that are meant to remain pattern free. After drying and removing the mask, the patterned circuits were immersed into a diluted HF solution for 30 min to completely remove the APTES and silica layer. After washing and drying, the uncured PDMS (601A/B) was carefully poured onto the patterned circuits and cured at room temperature. The PDMS layer was gently peeled off from the substrate to expose the embedded circuits. For the prestretched FSCs sample, the conductive patterns were embedded in the uncured PDMS (4600 A/B) before being transferred onto a prestretched PDMS (4600 A/B) substrate and cured at room temperature. To illustrate the electrical performance at bending, an array of LEDs was then assembled onto the top surface of the FSCs.

*Characterization*: The microstructure of the depositions was examined using TEM (FEI Tecnai, T20) and SEM (JEOL JSM-6301F). Fourier transform infrared spectroscopy (FT-IR, PerkinElmer, UATR Two) and XRD (Philips X'Pert Materials Research Diffractometer) were carried out to identify the surface functionalization of CNTs. The morphology of FSCs was observed using optical microscopy (Olympus, MX40). The dispersion quality of CNT-based hybrid nanowires in ethanol was characterized by UV–vis spectroscopy (UV–vis spectrometer, PerkinElmer, Lambda 900) with scanning wavelengths ranging from 200 to 700 nm and the intensity at the wavelength of 500 nm was chosen for measuring concentration variation. The electrical resistance of unstretched FSCs was measured by placing the sample on a probe station and using a four-probe method with probes heads (SUSS PH100). The resistance measurement of FSCs at different bending angles was carried out using the two-probe method by placing the samples against Teflon molds that were made into desired angles. The resistance difference between two probe and four probe measurement methods were found to be hardly noticeable in this work (<5%) due to the good contact of the hybrid nanowire-based FSCs with the metal probe pads. The electro-mechanical properties of FSCs during the cycled bending and stretching tests were measured by a high precision load/displacement measurement machine (Instron 5548 MicroTester), with the electrical multimeter's probes attached to the two grippers of the MicroTester. The conversion between sheet resistance and resistivity

during the stretching tests was calculated by optically measuring the change of trace width at the different strain levels. It was found that the variance of trace thickness is less than 5% within strain levels of 60%. Therefore, the trace thickness was kept constant and resistance was converted to sheet resistance and resistivity by using equations. $R = R_{sheet} \times$ (trace length/trace width), $R_{sheet} = \rho$/trace thickness. The reliability test of FSCs under deformation and the LED demonstrators were tested on the load/displacement machine at a strain rate of 5 mm $s^{-1}$.

## Supporting Information

Supporting Information is available from the Wiley Online Library or from the author.

## Acknowledgements

N.W. and D.J. contributed equally to this work. This work was supported by EU FP7 programs, "Nano-RF," "Nanotherm," and "Smartpower," Swedish Foundation for Strategic Research (SSF) Frame Project "Carbon-Based 3D High Speed GaN Electronics Systems" Contract No: SE13-0061 and SSF Project "Scalable Nanomaterials and Solution Processable Thermoelectric Generators," Contract No: EM11-0002. The authors also acknowledge financial support from The Production Area of Advance program, Chalmers University of Technology, Sweden, the National Chinese Science Foundation Project (51272153), The Shanghai Governmental Program (12JC1403900) as well as The Shanghai Jia Ding District.

Received: March 15, 2015
Revised: April 30, 2015
Published online: May 26, 2015

[1] J. Fjelstad, *Circuit World* **1999**, *25*, 6.
[2] S. Park, S. Jayaraman, *MRS Bull.* **2003**, *28*, 585.
[3] J. A. Rogers, Z. Bao, K. Baldwin, A. Dodabalapur, B. Crone, V. R. Raju, V. Kuck, H. Katz, K. Amundson, J. Ewing, P. Drzaic, *Proc. Natl. Acad. Sci. U.S.A.* **2001**, *98*, 4835.
[4] D. J. Lipomi, B. C.-K. Tee, M. Vosgueritchian, Z. Bao, *Adv. Mater.* **2011**, *23*, 1771.
[5] H. C. Ko, M. P. Stoykovich, J. Song, V. Malyarchuk, W. M. Choi, C. Yu, J. B. Geddes III, J. Xiao, S. Wang, Y. Huang, J. A. Rogers, *Nature* **2008**, *454*, 748.
[6] R. Carta, P. Jourand, B. Hermans, J. Thoné, D. Brosteaux, T. Vervust, F. Bossuyt, F. Axisa, J. Vanfleteren, R. Puers, *Sens. Actuators, A* **2009**, *156*, 79.
[7] T. Sekitani, T. Someya, *Adv. Mater.* **2010**, *22*, 2228.
[8] M. Gonzalez, F. Axisa, M. V. Bulcke, D. Brosteaux, B. Vandevelde, J. Vanfleteren, *Microelectron. Reliab.* **2008**, *48*, 825.
[9] X. Wang, H. Hu, Y. Shen, X. Zhou, Z. Zheng, *Adv. Mater.* **2011**, *23*, 3090.
[10] P. Calvert, *Chem. Mater.* **2001**, *13*, 3299.
[11] T. Dong, W. Chen, C. Wang, C. Chen, C. Chen, M. Lin, J. Song, I. Chen, T. Kao, *Phys. Chem. Chem. Phys.* **2009**, *11*, 6269.
[12] K. Kordás, T. Mustonen, G. Tóth, H. Jantunen, M. Lajunen, C. Soldano, S. Talapatra, S. Kar, R. Vajtai, P. M. Ajayan, *Small* **2006**, *2*, 1021.
[13] J. Wu, M. Agrawal, H. A. Becerril, Z. Bao, Z. Liu, Y. Chen, P. Peumans, *ACS Nano* **2010**, *4*, 43.
[14] L. Hu, H. S. Kim, J. Lee, P. Peumans, Y. Cui, *ACS Nano* **2010**, *4*, 2955.
[15] J. H. Byeon, J. Hwang, *Surf. Coat. Technol.* **2008**, *203*, 357.
[16] X. Ma, N. Lun, S. Wen, *Diamond Relat. Mater.* **2005**, *14*, 68.
[17] L. Zhao, L. Gao, *Colloids Surf., A* **2003**, *224*, 127.
[18] Y. Yamada, K. Yano, *Microporous Mesoporous Mater.* **2006**, *93*, 190.
[19] Z. Xiu, Y. Wu, X. Hao, L. Zhang, *Colloids Surf., A* **2011**, *386*, 135.
[20] F. Tang, L. Li, D. Chen, *Adv. Mater.* **2012**, *24*, 1504.
[21] S. K. Choi, K. Chun, S. Lee, *Diamond Relat. Mater.* **2009**, *18*, 637.
[22] X. Ma, N. Lun, S. Wen, *Diamond Relat. Mater.* **2005**, *14*, 68.
[23] S. Guo, J. Li, W. Ren, D. Wen, S. Dong, E. Wang, *Chem. Mater.* **2009**, *21*, 2247.
[24] Z. Chen, W. Ren, L. Gao, B. Liu, S. Pei, H.-M. Cheng, *Nat. Mater.* **2011**, *10*, 424.
[25] T. Kim, H. Song, J. Ha, S. Kim, D. Kim, S. Chung, J. Lee, Y. Hong, *Appl. Phys. Lett.* **2014**, *104*, 113103.
[26] T. Sekitani, Y. Noguchi, K. Hata, T. Fukushima, T. Aida, T. Someya, *Science* **2008**, *321*, 1468.
[27] S. Yun, X. Niu, Z. Yu, W. Hu, P. Brochu, Q. Pei, *Adv. Mater.* **2012**, *24*, 1321.
[28] K. Takei, Z. Yu, M. Zheng, H. Ota, T. Takahashi, A. Javey, *Proc. Natl. Acad. Sci. U.S.A.* **2014**, *111*,1703.
[29] F. Xu, Y. Zhu, *Adv. Mater.* **2012**, *24*, 5117.
[30] K. Chun, Y. Oh, J. Rho, J. Ahn, Y. Kim, H. R. Choi, S. Baik, *Nat. Nanotechnol.* **2010**, *5*, 853.
[31] M. Park, J. Im, M. Shin, Y. Min, J. Park, H. Cho, S. Park, M. Shim, S. Jeon, D. Chung, J. Bae, J. Park, U. Jeong, K. Kim, *Nat. Nanotechnol.* **2012**, *7*, 803.
[32] Y. Yu, J. Zeng, C. Chen, Z. Xie, R. Guo, Z. Liu, X. Zhou, Y. Yang, Z. Zheng, *Adv. Mater.* **2014**, *26*, 810.
[33] Y. Li, H. Shimizu, *Macromolecules* **2009**, *42*, 2587.
[34] L. Hu, M. Pasta, F. L. Mantia, L. Cui, S. Jeong, H. D. Deshazer, J. W. Choi, S. M. Han, Y. Cui, *Nano Lett.* **2010**, *10*, 708.
[35] J. Li, L. Liu, D. Zhang, D. Yang, J. Guo, J. Wei, *Synth. Met.* **2014**, *192*, 15.